

Article

Experimental Investigation on Behavior of Single-Helix Anchor in Sand Subjected to Uplift Cyclic Loading

Dongxue Hao ^{1,2,*}, Jianyi Che ², Rong Chen ^{1,2,*}, Xin Zhang ³, Chi Yuan ⁴  and Xichao Chen ²

¹ Key Lab of Electric Power Infrastructure Safety Assessment and Disaster Prevention of Jilin Province, Northeast Electric Power University, Jilin 132012, China

² School of Civil Engineering and Architecture, Northeast Electric Power University, Jilin 132012, China

³ Northeast Electric Power Design Institute Co., Ltd. of China Power Engineering Consulting, Changchun 130021, China

⁴ College of Architecture and Civil Engineering, Beijing University of Technology, Beijing 110124, China

* Correspondence: 20102291@neepu.edu.cn (D.H.); 20112384@neepu.edu.cn (R.C.);
Tel.: +86-432-6480-6481 (D.H.)

Abstract: Helical anchors have been widely used in geotechnical engineering due to their large uplift resistance. However, the current knowledge of the cyclic performance of helical anchors is still insufficient. Consequently, a series of small-scale model tests are carried out in sand to investigate the influences of embedment ratio, sand compactness and the cyclic parameters on the monotonic, cyclic and post-cyclic performance of single-helix anchors. The tests results indicate that the single-helix anchors with optimal embedment ratio still exhibit a relatively high uplift capacity after suffering cyclic load. The cyclic frequency has the greatest influence on the accumulated displacement, and the influence of amplitude is relatively greater than that of the mean cyclic load. The anchors in dense sand exhibit better performance to resist pullout than those in medium–dense sand under the same cyclic parameter ratios. Moreover, the correlation of post-cyclic uplift capacity and displacement after cyclic loading as well as the possible influence of the upward displacement on the sand flow above the helix are discussed.

Keywords: helical anchor; sand compactness; embedment ratio; cyclic uplift response; post-cyclic monotonic uplift capacity



Citation: Hao, D.; Che, J.; Chen, R.; Zhang, X.; Yuan, C.; Chen, X. Experimental Investigation on Behavior of Single-Helix Anchor in Sand Subjected to Uplift Cyclic Loading. *J. Mar. Sci. Eng.* **2022**, *10*, 1338. <https://doi.org/10.3390/jmse10101338>

Academic Editor: Erkan Oterkus

Received: 15 August 2022

Accepted: 18 September 2022

Published: 21 September 2022

Publisher's Note: MDPI stays neutral with regard to jurisdictional claims in published maps and institutional affiliations.



Copyright: © 2022 by the authors. Licensee MDPI, Basel, Switzerland. This article is an open access article distributed under the terms and conditions of the Creative Commons Attribution (CC BY) license (<https://creativecommons.org/licenses/by/4.0/>).

1. Introduction

Helical anchors or helical piles are widely used as foundations for various structures, such as transmission towers, onshore wind turbine foundations and floating offshore installations, to resist tension forces and vertical cyclic loads from wind, waves or current loads. They can provide large uplift capacity and good cyclic performance due to the anchor effect of the helix [1–5]. In recent years, this type of foundation has been suggested as a potential alternative to driven piles in offshore renewable energy structures due to the rapid installation, lesser disturbance, low noise and convenience for recycling [6,7].

The environmental cyclic loads are predominant in many applications of helical anchors, which need to be properly considered during design. The cyclic and post-cyclic responses of helical anchors with different geometries and the variations of loads the helix and shaft can resist during cyclic loading under different cyclic loading parameters and different loading sequences with different amplitudes in different soils have been investigated by 1 g model tests, centrifuge and field tests [8–20].

Clemence and Smithling [8] carried out the axial cyclic loading model test of single helical anchor in medium–dense sand to study the effects of displacement amplitude and pre-stressed load on the anchor response. The results show that the application of prestressed load can prolong the fatigue life of the anchor and the post-cyclic capacity decreases. Cerato and Buhler [9,10] and Buhler and Cerato [11] conducted field tests of

multi-helical anchors in layered soil to investigate the influence of the number of anchor plates, dynamic load application sequence, load characteristics and groundwater level fluctuations on the uplift behavior of helical anchors under long-term wind load, and validated the existing uplift bearing capacity prediction methods. They found that the triple-helical anchor has the best cyclic performance under long-term dynamic loading, while cyclic loads at 25–40% of the static uplift capacity may visibly increase the post-dynamic uplift capacity and minimize the long-term creep, while the amplitude of cyclic load has a greater influence on the dynamic response of the helical anchor than the maximum load. Sharnouby and Naggar [12,13] conducted field tests on steel fiber-reinforced helical pulldown micropiles under axial compressive cyclic loading to study the cyclic bearing characteristics and load transfer mechanism of piles under different loading sequences. Newgard et al. [14] performed static and cyclic loading tests on a helical anchor model at shallow embedment in saturated medium–dense sand and observed the rapid increase in the rate of accumulation of displacements when the anchor reaches the displacement near the peak static load and the degradation of post-cyclic capacity. Wada et al. [15] investigated the bearing and pullout capacities of steel piles with continuous helix wings under two-way stepwise cyclic loading with an increment of 1/6 of ultimate static capacity for every three cycles by laboratory and field tests. It was found that the bearing and pullout capacities of continuous helix piles under cyclic reversal loading decreased to approximately 60–80% of those under monotonic loading, and the decrease in resistance was mainly due to the reduction in shaft friction. Schiavon et al. [16,17] carried out centrifugal tests for cyclic and post-cyclic monotonic loading of single-helix anchors in very dense sand. The results indicated that a rapid degradation of shaft resistance occurred during cyclic loading, no or slight reduction of post-cyclic uplift capacity occurred for stable anchors, cumulative permanent displacements developed rapidly in the approximately first 100 cycles and previous large cyclic amplitude improved the anchor cyclic performance. Schiavon et al. [18] also performed field tests for single-helix anchors in residual soil of sandstone. The results of cyclic loading tests show no significant degradation of helix bearing resistance and reduced displacement accumulation with increasing load cycles during the first stage cyclic loading. Thorel et al. [19] investigated the effect of the installation rotation rate on the tension resistance and the behavior of helical pile under cyclic loading based on centrifuge models. Hao et al. [20] investigated the influence of embedment ratio of single-helix anchor and number of helices on the cyclic uplift capacity in dense sand by centrifugal stepwise cyclic uplift tests. They found that the ultimate cyclic loading level increases gradually with embedment ratio to the maximum value at the embedment ratio of 6, and then keeps almost constant for greater embedment ratios. The uplift displacements at the beginning of ultimate cyclic loading level are very close to the failure displacements under monotonic loading for single-helix anchors. In addition, the double-helix anchor accumulates less uplift displacement than the single-helix anchor during cyclic loading.

Although these previous studies provided important information, the current knowledge of the cyclic performance of helical piles is still insufficient to enable the development of an appropriate design procedure [16]. Additionally, the influences of sand compactness and frequency on the performance of helical anchors under cyclic loading, as well as the possible change rule of sand compactness with anchor displacement after cyclic loading are rarely reported in the previous literature. Therefore, more investigations on the cyclic behavior of helical piles are necessary to confirm the findings of the previous studies, and to provide new results for onshore and offshore applications [1].

This paper carried out monotonic and cyclic loading model tests of single-helix anchors in medium–dense sand and dense sand to investigate the development of accumulated displacement, axial cyclic stiffness and post-cyclic uplift capacity. It focused on the comprehensive effects of embedment ratio on accumulated displacement, static and post-cyclic ultimate uplift capacity, and the differences in the development of accumulated displacement, axial stiffness and the post-cyclic uplift capacity ratio in different sand compactness under various cyclic loading conditions.

2. Materials and Methods

2.1. Sand Preparation and Installation of Anchors

The silica sand sample was prepared by the air pluviation method in a rectangular strongbox with internal dimensions of 1000 × 500 × 1000 mm (length × width × depth). The particle size of the sand is in between 0.1 and 1 mm, and the particle size in the range of 0.25–0.5 mm accounts for 89.5% of the total mass. The properties of the silica sand are given in Table 1.

Table 1. Properties of silica sand.

Property	Value
Specific gravity, G_s	2.63
Average grain size d_{50} : mm	0.35
Coefficient of uniformity, C_u	1.57
Curvature coefficient, C_c	0.96
Maximum dry density, ρ_{dmax} (g/cm ³)	1.75
Minimum dry density, ρ_{dmin} (g/cm ³)	1.55
Critical friction angle, ϕ_{cv} (°)	28

Dry sand samples with relative density $D_r = 62\%$ (medium–dense sand) and $D_r = 92\%$ (dense sand) were obtained, respectively, by controlling the height, travel speed and opening width of the sand rain. The helical anchors are made of stainless steel. The thickness of the anchor plate is 1 mm and the diameter of the anchor plate D is 50 mm. The pitch and rod diameter are determined by referring to the size proportion of the helical anchor RS series products of A.B Chance [21]. The ratio of rod diameter to plate diameter $d/D = 0.25$, and the ratio of pitch to plate diameter $t/D = 0.3$. The helical plate and each rod part can be connected by screws and the base of the anchor is conical. The single-helix anchor models were installed by manually turning the handle at the speed of 20 rpm (80 mm/min). Anchor models and torsion mounting bracket are shown in Figure 1. Two anchors are installed in one strongbox. The distance between the two anchors is $8D$ and the minimum distance between the anchor and the wall of the box is $5D$, which meets the requirements of boundary conditions [22]. Figure 2 shows the process of sand preparation and installation of anchors, as well as the connection with MTS actuator.



Figure 1. Model of helical anchor and torsion mounting frame.



Figure 2. Sand preparation, installation and connection with actuator of anchors.

2.2. Test Program and Loading Mode

In order to analyze the influence of anchor depth, cyclic loading parameters and sand compactness on the cyclic performance of helical anchors, four groups of comparative tests are designed, as shown in Table 2. The cyclic loading pattern is shown in Figure 3. The anchors were pulled monotonically to the mean cyclic load Q_{mean} first, and then vibrated for 1200 cycles in a one-way sinusoidal cyclic manner. The mean cyclic load Q_{mean} and amplitude Q_{cyc} are both set according to the ratio of static ultimate uplift capacity Q_t that is obtained from the monotonic pull-out test of another anchor in parallel with the cyclic loading test. The maximum mean cyclic load Q_{mean} is taken as $0.5Q_t$ considering the design safety factor of 2 for static loading, while the amplitude Q_{cyc} varies from $0.1-0.3 Q_t$. Cyclic frequency f is set 0.5 Hz, and when comparing the effect of frequency, f is set 1 Hz and 2 Hz. The anchors that are still stable after vibration are subjected to monotonic pull-out load to determine the post-cyclic uplift capacity Q_{pt} . The testing program encompasses 28 monotonic and cyclic tests across 15 sand samples. The first letter of the test name represents the loading mode, i.e., M represents monotonic loading and C stands for cyclic loading; the second letter represents the compactness of sand samples, i.e., D for dense sand and M for medium-dense sand; the third letter H and the number close to H represents the embedment ratio, and the number after “-” is the number of parallel tests; the figures in brackets are the relative mean cyclic load Q_{mean}/Q_t and the relative amplitude Q_{cyc}/Q_t in turn. For the test on the effect of frequency, the frequency is listed last, and the ones unlisted are 0.5 Hz.

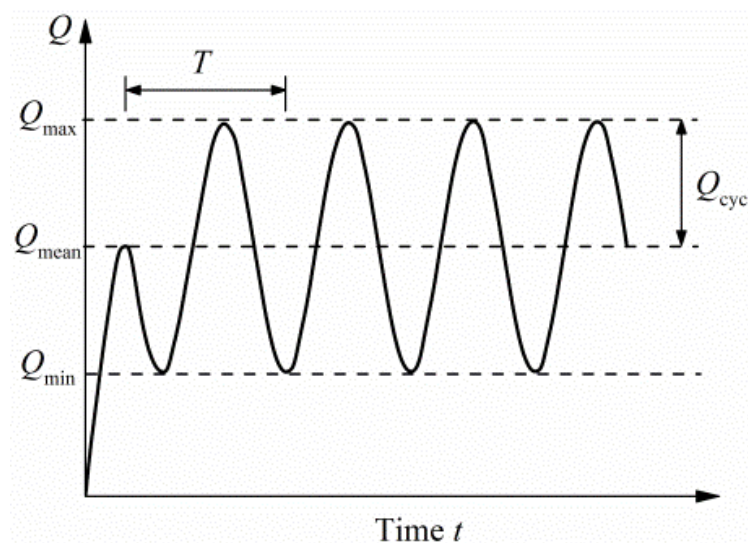


Figure 3. Pattern of cyclic loading.

Table 2. Test program.

Name	Sand Sample	Influence Factor	Frequency f/Hz	H/D	$\frac{Q_{\text{mean}}}{Q_t}$	$\frac{Q_{\text{cyc}}}{Q_t}$	Number of Cycles	Q_t/N	Uplift Capacity Ratio, β
MDH8	1		—	8	—	—	—	316.3	—
CDH8 (0.4, 0.2)	1		0.5	8	0.4	0.2	1200	318.5	1.007
MDH10	2		—	10	—	—	—	580.1	—
CDH10 (0.4, 0.2)	2	depth	0.5	10	0.4	0.2	1200	439.6	0.758
MDH12-1	3		—	12	—	—	—	863.3	—
CDH12 (0.4, 0.2, 0.5 Hz)	3		0.5	12	0.4	0.2	1200	850.6	0.985
MDH14	4		—	14	—	—	—	890.3	—
CDH14 (0.4, 0.2)	4		0.5	14	0.4	0.2	1200	733.9	0.824
MDH12-2	5		—	12	—	—	—	822.3	—
CDH12 (0.4, 0.3)	5		0.5	12	0.4	0.3	14	—	—
MDH12-3	6	cyclic amplitude and mean load	—	12	—	—	—	802.2	—
CDH12 (0.3, 0.3)	6		0.5	12	0.3	0.3	1200	876.7	1.093
CDH12 (0.4, 0.1)	7		0.5	12	0.4	0.1	1200	679.7	0.847
CDH12 (0.3, 0.2)	7		0.5	12	0.3	0.2	1200	780.5	0.973
CDH12 (0.2, 0.2, 0.5 Hz)	8		0.5	12	0.2	0.2	1200	738.3	0.920
CDH12 (0.5, 0.1)	8		0.5	12	0.5	0.1	1200	805.8	1.004
MDH12-4	9	frequency	—	12	—	—	—	813.2	—
CDH12 (0.4, 0.2, 1 Hz)	9		1	12	0.4	0.2	12	—	—
MDH12-5	10		-	12	-	-	-	803.8	—
CDH12 (0.2, 0.2, 2 Hz)	10		2	12	0.2	0.2	526	808.5	1.006
MMH12-1	11	compactness	—	12	—	—	—	658.8	—
CMH12 (0.3, 0.1)	11		0.5	12	0.3	0.1	1200	570.7	0.866
MMH12-2	12		—	12	—	—	—	638.4	—
CMH12 (0.3, 0.2)	13		0.5	12	0.3	0.2	1200	655.0	1.026
MMH12-3	14		—	12	—	—	—	630.4	—
CMH12 (0.3, 0.3)	14		0.5	12	0.3	0.3	1200	521.3	0.827
CMH12 (0.2, 0.2)	15		0.5	12	0.2	0.2	1200	620.5	0.984
CMH12 (0.4, 0.2)	15		0.5	12	0.4	0.2	1200	623.6	0.989

The monotonic and cyclic loading of the helical anchor is realized by MTS hydraulic actuator. The anchor head is rigidly connected with the actuator, as shown in Figure 2. Monotonic loading is controlled by displacement at the rate of 0.125 mm/s, and the pullout displacement is $1D$. Cyclic loading is applied according to the set load parameters. After cyclic loading, displacement control is used for monotonic pullout of the helical anchors. The data acquisition frequency is 12.8 Hz.

3. Results

3.1. Test Results in Dense Sand

3.1.1. Results of Anchors with Different Embedment Ratios

- Ultimate uplift capacity of monotonic loading

In order to analyze the influence of the embedment ratio on the monotonic and cyclic uplift behavior of helical anchors in dense sand, the tests of anchors with embedment ratio H/D varying from 8 to 14 were carried out with a fixed vibration frequency of $f = 0.5$ Hz, a mean cyclic load ratio $Q_{\text{mean}}/Q_t = 0.4$ and amplitude ratio $Q_{\text{cyc}}/Q_t = 0.2$.

Figure 4 shows the ultimate uplift capacity Q_t and the breakout factor N_γ of helical anchors with various embedment ratios under monotonic loading, where $N_\gamma = Q_t/\gamma AH$, among which Q_t is the peak values before the load displacement curve exhibits an obvious oscillation, as listed in Table 2; γ is the unit weight of soil mass; A is the cross-sectional area of anchor plate and H is the embedment depth of anchor plate. It can be seen that the static ultimate uplift capacity Q_t increases with the increase in embedment ratio H/D , and when $H/D \geq 12$, the growth rate of Q_t slows down. The N_γ reaches the maximum at

$H/D = 12$, beyond which the anchor can be considered as deeply buried [22,23]. The smaller the compactness of the sand sample, the smaller the critical embedment ratio corresponding to deep anchor [23,24]. Therefore, the embedment ratio of 12 can ensure that the anchor is deeply buried for medium–dense sand.

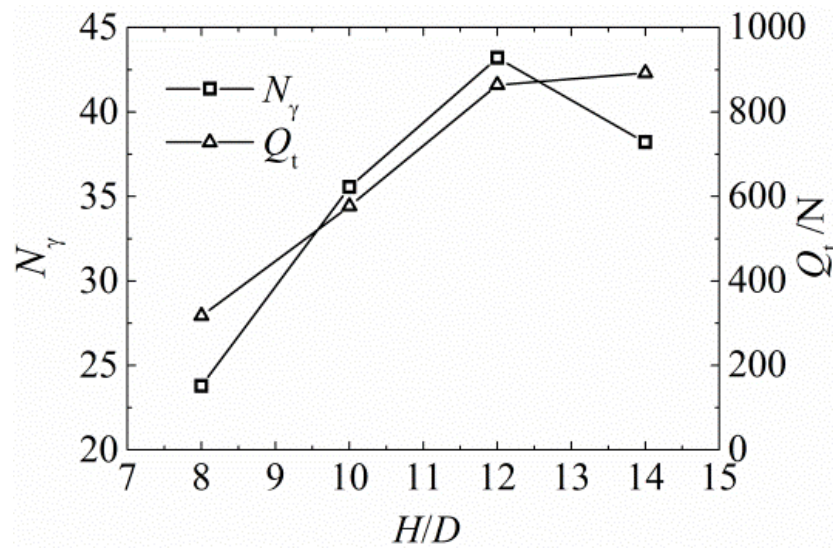


Figure 4. N_γ and Q_t of helical anchors with different embedment ratios in dense sand.

Figure 5 shows the standardized load and displacement curve $u/D-Q/Q_t$ under cyclic loading with different embedment ratios. The results of the first six cycles are shown in Figure 5b to demonstrate the loading process. There is an error between the actually applied load and the target load during the first three cycles. The applied load is slightly smaller than the target load when the embedment ratio H/D equals 8 due to the relative small cyclic load and the loading accuracy of the actuator.

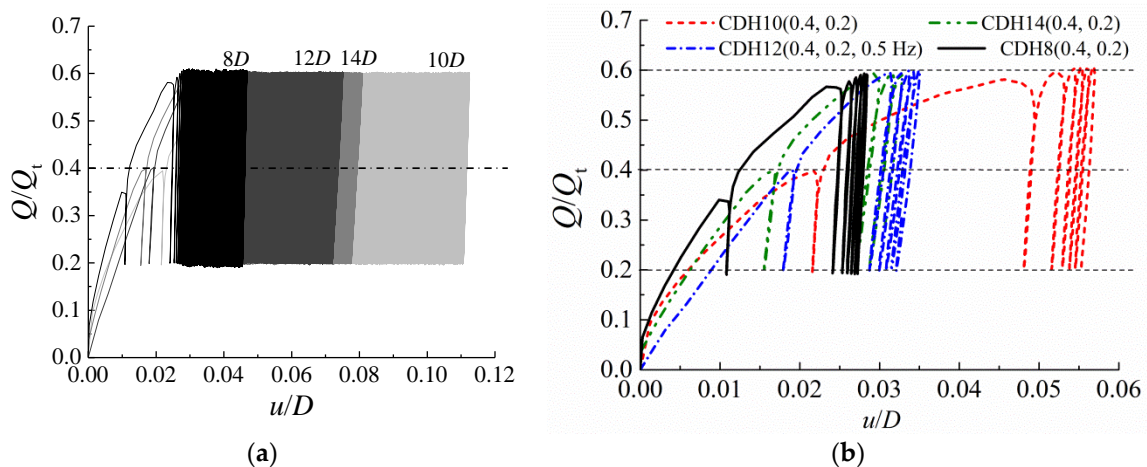


Figure 5. Standardized load–displacement curves at different embedment ratios (a) $N = 1200$; (b) $N = 6$.

Figure 6 shows the relationship between the number of cycles and standardized displacement, including the initial monotonic uplift displacement u_0 at $Q = 0.4Q_t$. The values of u_0 of the anchors with the embedment ratio $H/D = 8, 10, 12$ and 14 are $0.01D, 0.022D, 0.02D$ and $0.016D$, respectively. The value of u_0 for anchor CDH8 (0.4, 0.2) is smaller than that of the other cases, which may be related to the fact that the initial monotonic loading $Q = 0.35Q_t$ does not reach the standard of $0.4Q_t$. Additionally, the value of u_0 for anchor CDH10 (0.4, 0.2) is the largest, which may be due to the initial difference of

sand samples or installation disturbance. The standardized pullout displacements u/D for the anchors with various embedment ratios after cyclic loading are less than 0.1, with the exception of CDH10 (0.4, 0.2).

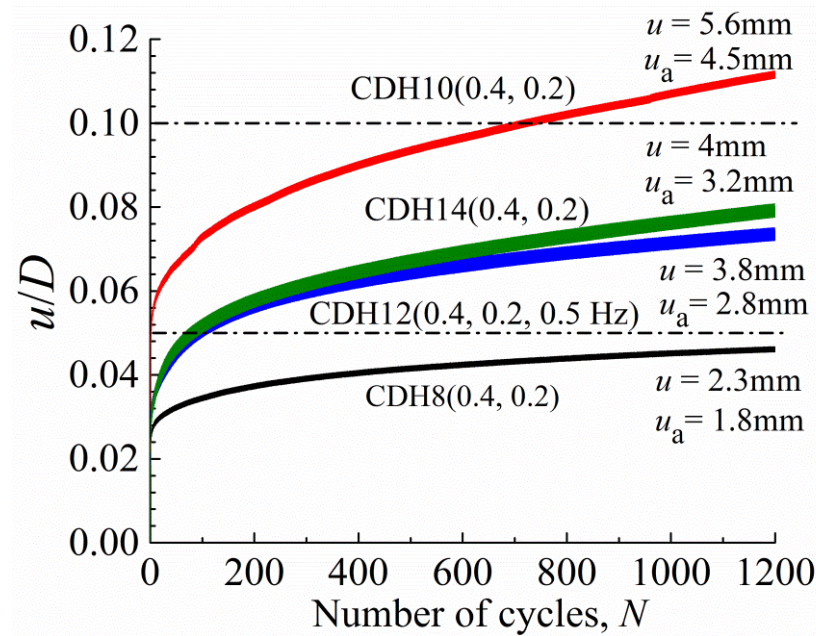


Figure 6. Developments of uplift displacement at different embedment ratios.

- Accumulated displacement

The developments of accumulated displacement u_a and displacement accumulation rate with number of cycles N for the anchors with different embedment ratios are plotted in Figure 7. The displacement accumulation rate is the accumulated displacement in each cycle. It can be seen from Figure 7a that u_a increases nonlinearly when $N < 200$ and then develops in a linear and slow way. The accumulated displacement of anchor CDH8 (0.4, 0.2) is the smallest, which may be related to the relatively small amplitude of the anchor and the first few cyclic loads being less than the target value compared to other anchors. Anchor CDH12 (0.4, 0.2, 0.5 Hz) shows better cyclic performance than anchor CDH10 (0.4, 0.2) and CDH14 (0.4, 0.2). Figure 7b displays the semi-log relationships of u_a and N , which are linear before exhibiting hollow circles and then develops nonlinearly in different extents. The values of u_a at the hollow circles are close to $0.02D$, except for CDH10 (0.4, 0.2), and the numbers of cycles corresponding to hollow circles are less than 50 for all anchors with different embedment ratios. The values of accumulated displacement at $N = 50$ are all more than half of the total accumulated displacement, which indicates that the accumulated displacement develops significantly before $N = 50$.

It can be seen from Figure 7c that the accumulated displacement in the first cycle for the anchor CDH10 (0.4, 0.2) is 1.9–2.6 times that of other anchors with different embedment ratios, which may be due to the effect of installation disturbance. The initial displacement accumulation rate is the largest, and then decreases rapidly within three cycles, until reaching a small and stable value after 10 cycles for the anchors with different embedment ratios. The displacement accumulation rate decreases from 0.91–1.82 mm/10 cycles at the first 10 cycles to 0.14–0.3 mm/100 cycles after 100 cycles.

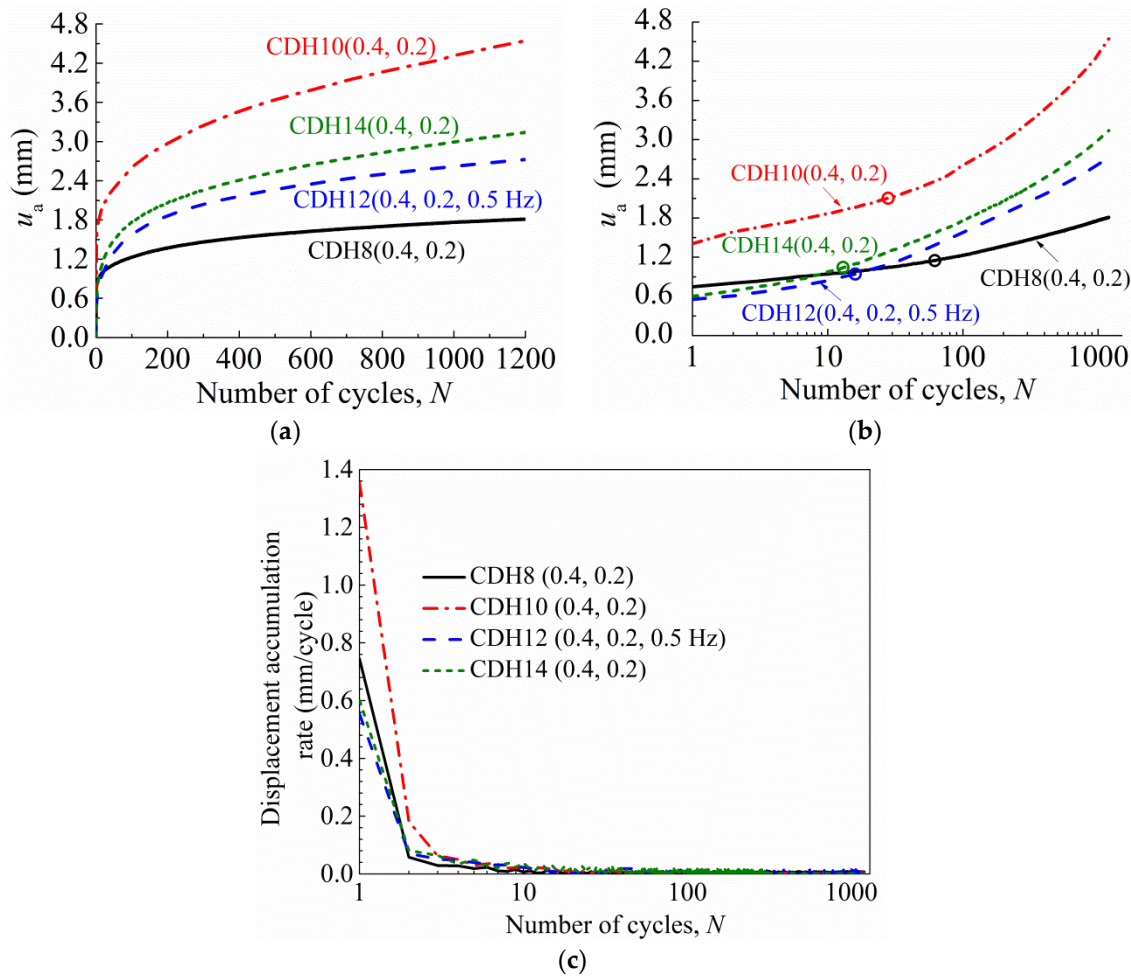


Figure 7. Developments of accumulated displacement and displacement accumulation rate at different embedment ratios: (a) linear scale of u_a-N ; (b) semi-log scale of u_a-N ; (c) semi-log scale of displacement accumulation rate and cycle number.

- Axial stiffness

The axial stiffness k of the helical anchor is defined by the ratio of the load increment in each loading cycle to its deformation increment, as shown in Figure 8a. The relationships of axial stiffness k and normalized axial stiffness k_N/k_1 with number of cycles N for different embedment ratios are plotted in the semi logarithmic coordinate system, as shown in Figure 8b,c, where k_N and k_1 are the axial stiffness of the N^{th} cycle and the first cycle, respectively.

It can be seen from the figure that the axial stiffness k increases rapidly and nonlinearly within 10 cycles for different embedment ratios. The developments of axial stiffness for anchor CDH8 (0.4, 0.2) and CDH10 (0.4, 0.2) are generally stable after 10 cycles, although there are slight fluctuations compared to the other two anchors. The stiffness of the first two cycles is relatively low for CDH10 (0.4, 0.2) due to the sand loosening, which is caused by installation disturbance, and then the stiffness increases rapidly when the vibration densifies the sand above the anchor. The stable values of axial stiffness for anchor CDH8 (0.4, 0.2), CDH10 (0.4, 0.2), CDH12 (0.4, 0.2, 0.5 Hz) and CDH14 (0.4, 0.2) are 10.5 times, 13.9 times, 4.4 times and 4.3 times of the initial axial stiffness, respectively.

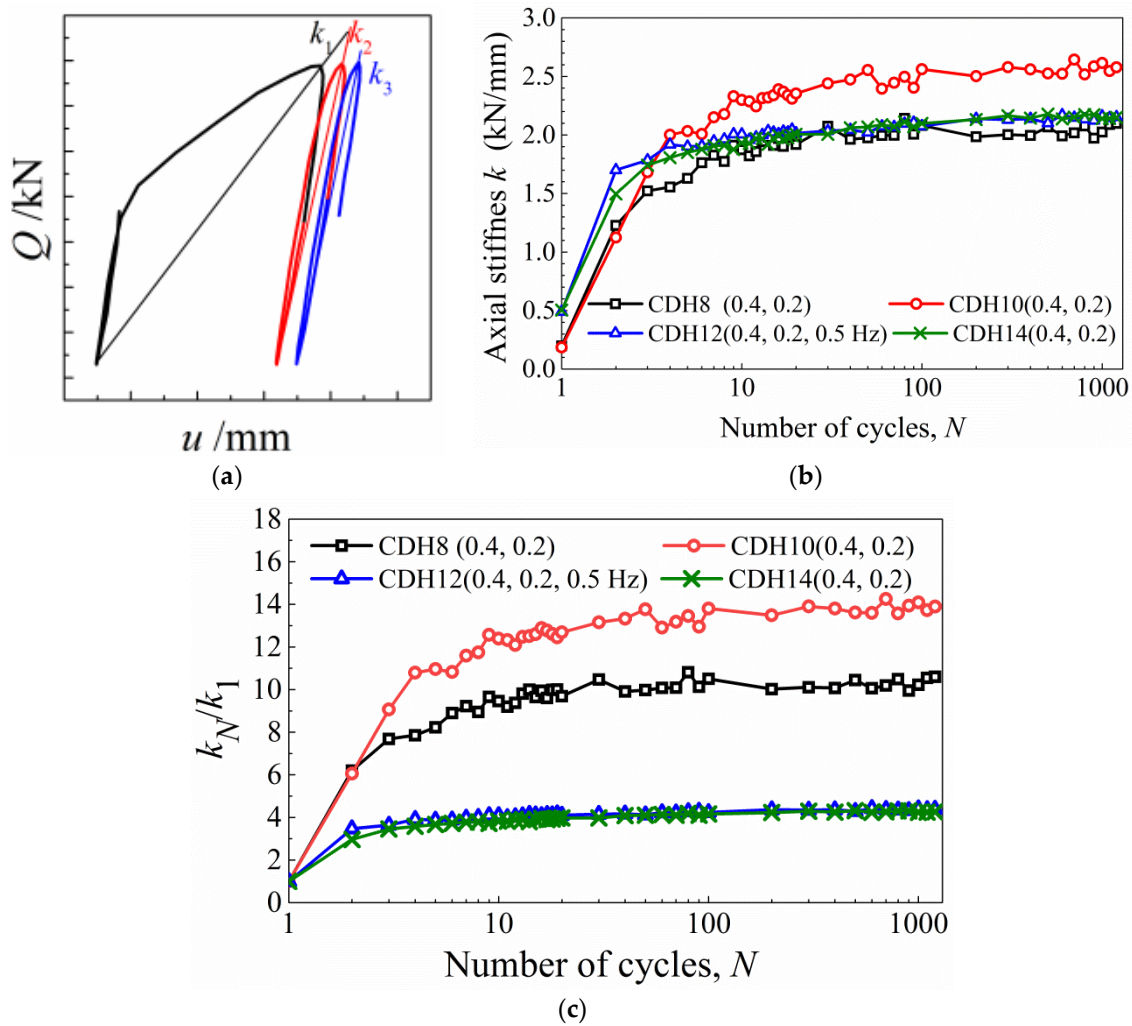


Figure 8. Axial stiffness for different embedment ratios: (a) definition of axial stiffness; (b) relationship of axial stiffness k and number of cycles N ; (c) relationship of normalized axial stiffness k_N/k_1 and number of cycles N .

- Post-cyclic monotonic response and uplift capacity

The monotonic pull-out tests were carried out after cyclic loading to obtain the load displacement responses, which were compared with the results of monotonic tests without cyclic loading, as shown in Figure 9, where the peak points are marked in the grey circles.

It can be seen from the figure that the monotonic responses after cyclic loading for the helical anchors with different embedment ratios are more rigid than that without cyclic loading. When monotonic pullout is carried out directly, the peak points of each anchor appear after the uplift displacement of $0.1D$, while the peak points after cyclic loading are reached before $0.1D$. Schiavon et al. [17] also found the stiffer initial response in post-cyclic monotonic uplift test by centrifuge and the peak points of direct monotonic and post-cyclic monotonic pullout also occur after and before uplift displacement of $0.1D$, respectively.

The uplift capacity ratio after cyclic loading β is defined as the ratio of ultimate uplift capacity after cyclic loading Q_{pt} and static ultimate uplift capacity Q_t . The values of β for anchor CDH8 (0.4, 0.2), CDH10 (0.4, 0.2), CDH12 (0.4, 0.2, 0.5 Hz) and CDH14 (0.4, 0.2) are 1.007, 0.756, 0.985 and 0.824, respectively, which indicates that the ultimate uplift capacities of helical anchors with different embedment ratios in dense sand after cyclic loading with cyclic parameters (0.4, 0.2, 0.5 Hz) are not improved, and in fact some of them significantly reduced. The influence of the embedment ratio on the post-cyclic uplift capacity of anchors is irregular.

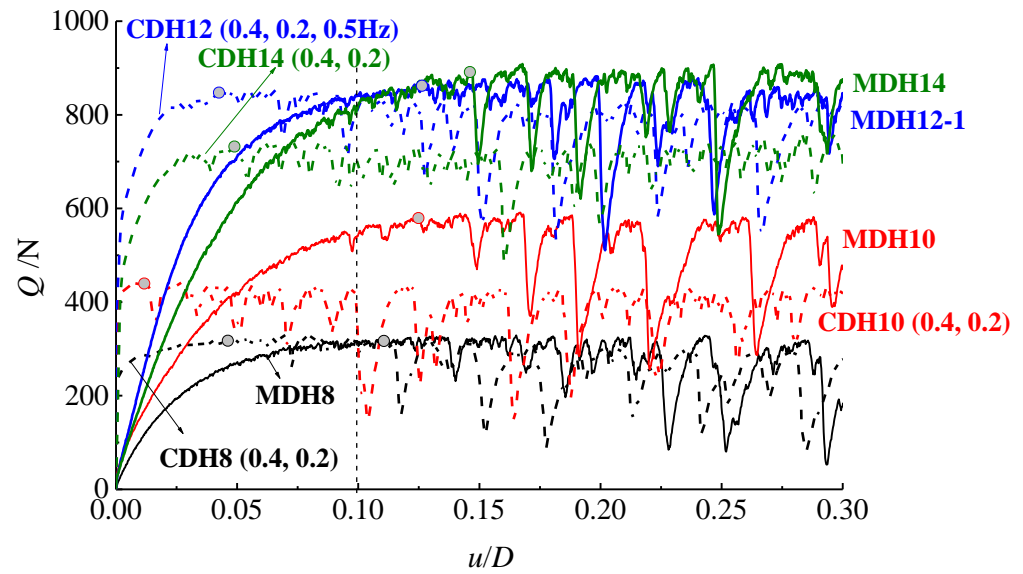


Figure 9. Post-cyclic monotonic and monotonic responses for different embedment ratios.

The single-helix anchor test with the embedment ratio of 12 exhibits the good static and cyclic behavior based on post-cyclic uplift capacity and the development of cyclic accumulated displacement and axial stiffness. Therefore, the helical anchor with $H/D = 12$ is selected for the later tests.

3.1.2. Results for Different Amplitudes and Mean Cyclic Loads

- Accumulated displacement

Figure 10 shows the accumulated displacement developments of the anchors under different amplitudes ($f = 0.5$ Hz and $Q_{mean}/Q_t = 0.4$ and 0.3). It is evident that the greater the amplitude, the greater the accumulated displacement u_a when other cyclic parameters are the same, which is similar with the observation of Hanna et al. [25] and Petereit [26] for plate anchors and Schiavon et al. [16,17] for helical anchors. The u_a increases non-linearly and rapidly for N less than 200 and then develops slowly under the situation of $Q_{max} = Q_{mean} + Q_{cyc} < 0.7Q_t$, while u_a develops very fast with cycle number and has reached $0.8D$ after 14 cycles when Q_{mean}/Q_t equals 0.4 and Q_{cyc}/Q_t equals 0.3 ($Q_{max} = 0.7Q_t$), which is likely to represent a continuously pulled out case for which the test is interrupted.

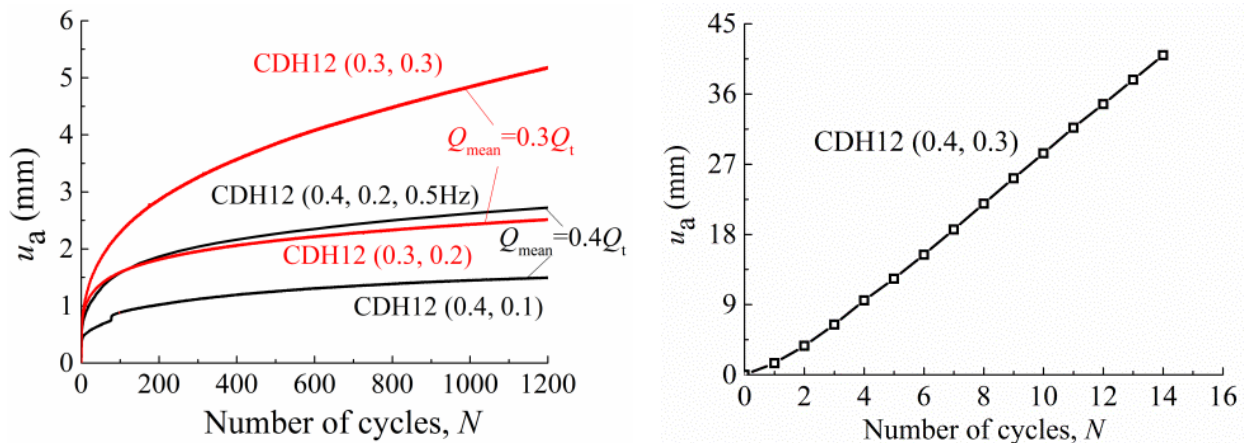


Figure 10. Developments of accumulated displacement under different amplitudes.

The curves of accumulated displacement u_a with cycle number N for the anchors subjected to different mean cyclic load ratios Q_{mean}/Q_t and the same amplitude ratios Q_{cyc}/Q_t of 0.1 or 0.2 are plotted in Figure 11. When Q_{cyc}/Q_t equals 0.2 and Q_{mean}/Q_t varies from 0.2 to 0.4, the rule according to which the greater the mean cyclic load, the larger accumulated displacement is observed. While when Q_{cyc}/Q_t equals 0.1, the accumulated displacement of anchor CDH12 (0.5, 0.1) subjected to a mean cyclic load ratio of 0.5 is obviously smaller than that of anchor CDH12 (0.4, 0.1) with a mean cyclic load ratio of 0.4, which is similar to the results of the sequence cyclic loading tests for single-helix anchors from Schiavon et al. [17] where a subsequent low-level cyclic loading produces very low permanent displacements due to the anchor performance being improved by previous large amplitude cyclic-loading. The observation indicates that the influence of the mean cyclic load on the accumulated displacement may be affected by the amplitude. When the amplitude is medium, the accumulated displacement of anchors subjected to a greater mean cyclic load will be larger. Additionally, when the amplitude is small, the influence of the mean cyclic load on the accumulated displacement shows the opposite trend. This phenomenon may be due to the fact that the sand densification above the anchor caused by preloading will remain dense during small amplitude cyclic loading, and the sand densification by preloading cannot be sustained and eventually becomes loose due to the backflow of sand above the anchor under the larger maximum cyclic load (corresponding to medium amplitude). The relationship of the accumulated displacement between anchor CDH12 (0.3, 0.2) > CDH12 (0.4, 0.1) and anchor CDH12 (0.3, 0.3) > CDH12 (0.4, 0.2, 0.5 Hz) > CDH12 (0.5, 0.1) can be observed by comparing the accumulated displacement of the anchors with the same maximum cyclic load ratio Q_{max}/Q_t . This indicates that for the anchors under the same maximum cyclic load ratio Q_{max}/Q_t , the greater accumulated displacement will be obtained when the anchors are subjected to the larger value of Q_{cyc}/Q_t and the smaller value of Q_{mean}/Q_t . The same conclusion for single-helix anchors in very dense sand is obtained by Schiavon et al. [17].

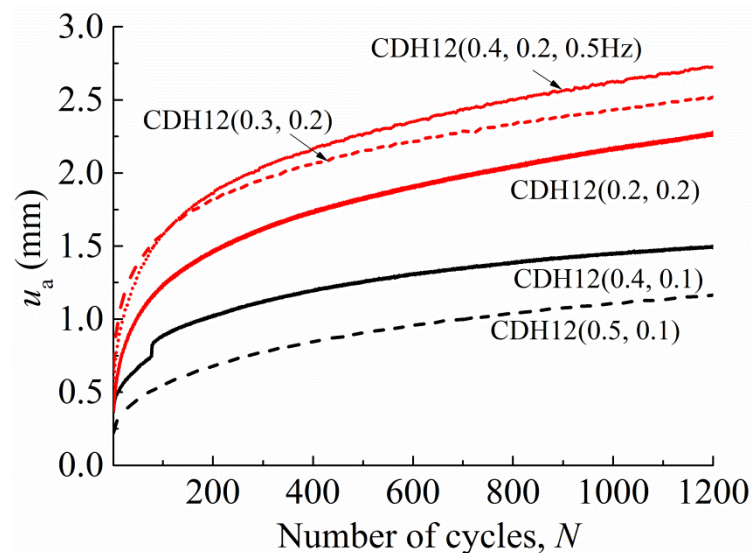


Figure 11. Developments of accumulated displacement under different mean cyclic loads.

The developments of displacement accumulation rate of the anchors under different amplitudes and mean cyclic loads are shown in Figure 12. The rules of development for all the anchors are similar. The displacement accumulation rate decreases rapidly within three cycles, and then decreases slowly when the cycle number is more than 3 and less than 10. However, there is still an oscillated displacement accumulation rate after 100 cycles, which decreases to 0.1–0.23 mm per 100 cycles.

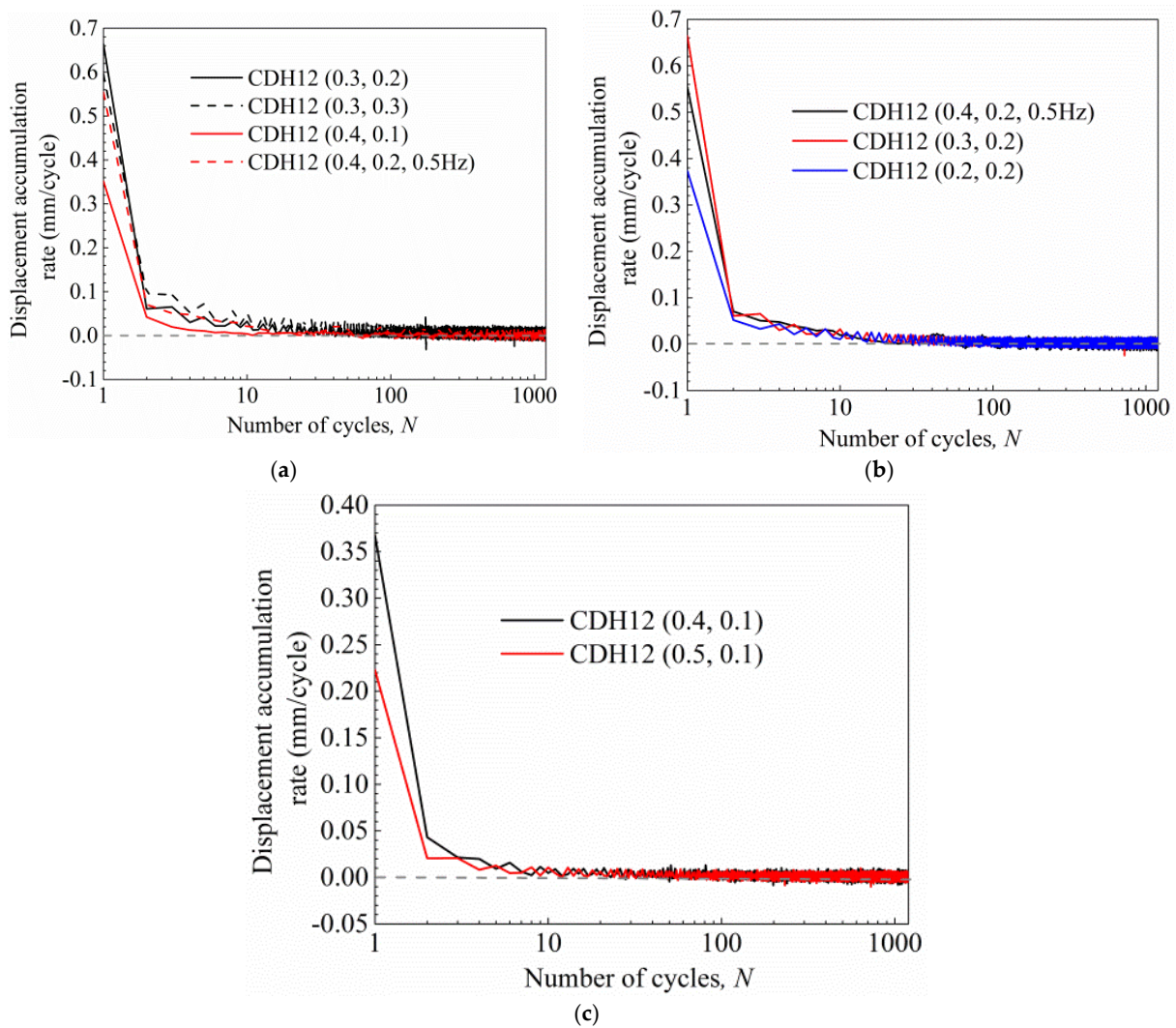


Figure 12. Developments of displacement accumulation rate under different amplitudes and mean loads: (a) the influence of amplitude; (b) the influence of mean cyclic load $Q_{cyc}/Q_t = 0.2$; (c) the influence of mean cyclic load $Q_{cyc}/Q_t = 0.1$.

The anchor under the greater amplitude has the larger displacement accumulation rate, and the phenomenon is more obvious for larger Q_{mean} . The displacement accumulation rate of anchors under small mean cyclic loads is relatively small in the cases of the same medium amplitude, and the displacement accumulation rate of the anchor under a smaller mean cyclic load is larger in the cases of the same small amplitude.

- Axial stiffness

The relationships between axial stiffness and the number of cycles for the anchors in dense sand subjected to different Q_{mean}/Q_t and Q_{cyc}/Q_t are shown in Figure 13, which shows similar behaviors. The axial stiffness increases with the cycle number rapidly and nonlinearly within ten cycles and reaches stability at cycle numbers between 10 and 50. Stable axial stiffness is about three to six times the initial value for all the cases of different Q_{mean}/Q_t and Q_{cyc}/Q_t , except for CDH12 (0.4, 0.3). It is observed that the axial stiffness for anchors under a larger amplitude is relatively small and has no significant correlation with the mean cyclic load.

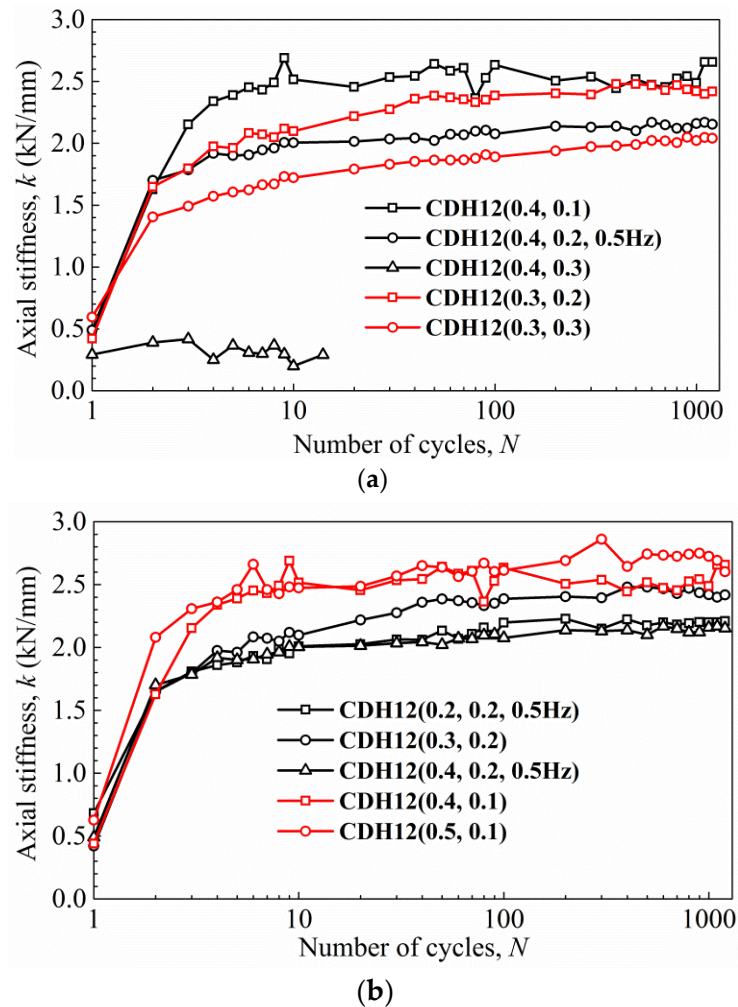


Figure 13. Developments of axial stiffness for different amplitudes and mean cyclic loads: (a) different amplitudes; (b) different mean cyclic loads.

- Post-cyclic monotonic response and uplift capacity

Figure 14 shows the monotonic responses of anchors without cyclic loading and post-cyclic monotonic responses in dense sand. The uplift capacity ratios after cyclic loading β for anchor CDH12 (0.4, 0.2, 0.5 Hz) and CDH12 (0.4, 0.1) are 0.985 and 0.847, respectively. Additionally, the values of β for anchor CDH12 (0.3, 0.2) and CDH12 (0.3, 0.3) are 0.973 and 1.093, respectively. The anchors subjected to a greater amplitude have a higher post-cyclic uplift capacity when the same mean cyclic loads are applied. The values of β vary from 0.847 to 1.004 when the amplitude ratio $Q_{cyc}/Q_t = 0.1$ and 0.2, and the mean cyclic load ratio $Q_{mean}/Q_t = 0.2-0.5$. Among these anchors, CDH12 (0.3, 0.3) has the largest displacement after cyclic loading, CDH12 (0.5, 0.1) has the smallest displacement and both uplift capacity ratios are greater than 1. Additionally, the centrifuge test results from Schiavon et al. [17] show the slight post-cyclic capacity degradation of 1–7% for the cases of $Q_{max}/Q_t = 0.42-0.69$, while the centrifuge test results from Schiavon et al. [16] show no reduction or a slight increase in post-cyclic capacity for the $Q_{max}/Q_t = 0.61-0.93$. The ratio of Q_{max}/Q_t used in this study is similar to that in Schiavon et al. [17]; however, both a decrease and increase in the post-cyclic capacity occur, and the variation of post-cyclic capacity in comparison with monotonic value range from -15% to 10% .

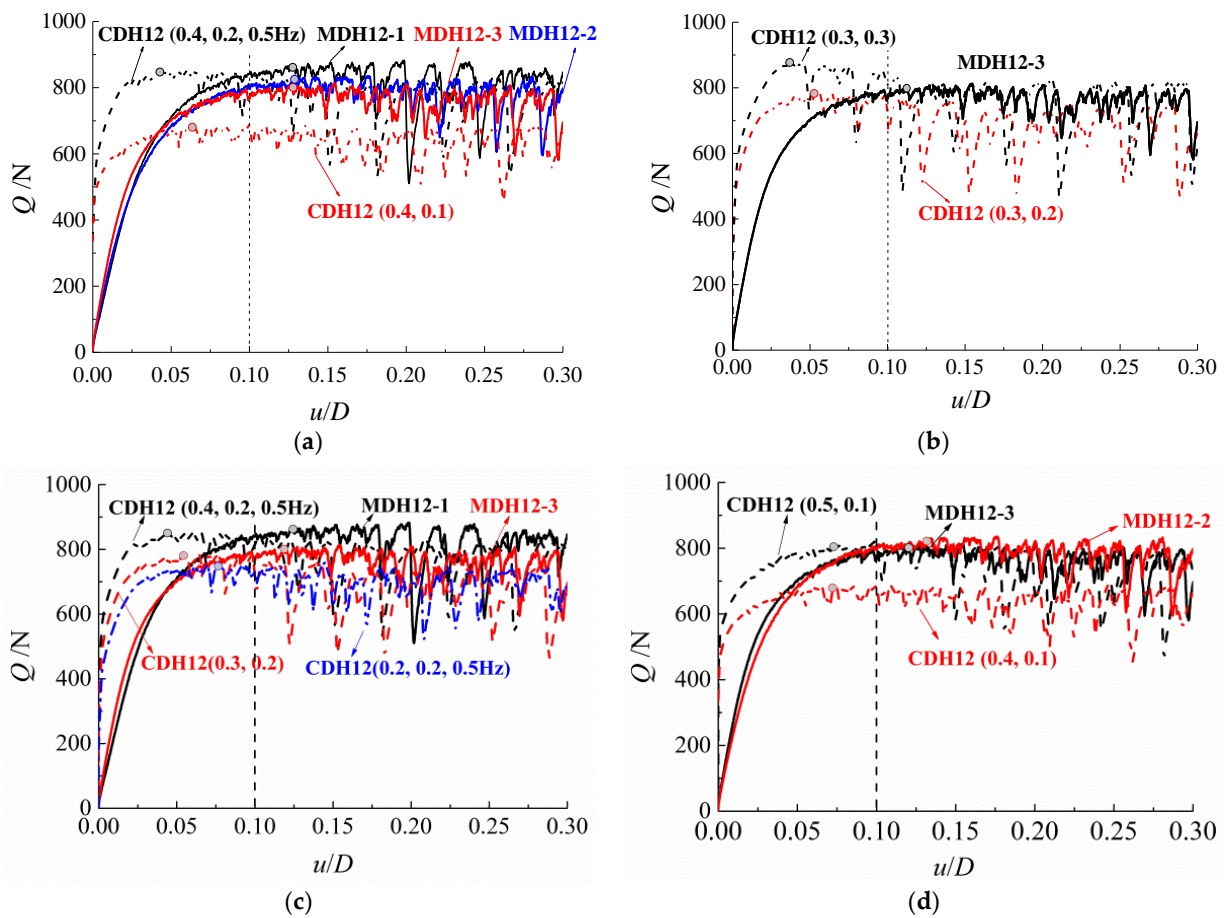


Figure 14. Monotonic and post-cyclic monotonic responses for different amplitudes and mean cyclic loads: (a) $Q_{mean}/Q_t = 0.4$; (b) $Q_{mean}/Q_t = 0.3$; (c) $Q_{cyc}/Q_t = 0.2$; (d) $Q_{cyc}/Q_t = 0.1$.

3.1.3. Results for Different Cyclic Loading Frequencies

The developments of accumulated displacement under different cyclic frequencies are shown in Figure 15. Anchor CDH12 (0.4, 0.2, 1 Hz) under a frequency of 1 Hz is pulled up sharply at the initial stage of cyclic loading, indicating that the vibration frequency is close to the natural frequency of the anchor–soil system, and resonance occurs. The test is stopped when cyclic loading is applied for 12 cycles. Comparing the accumulated displacement development of CDH12 (0.2, 0.2, 0.5 Hz) and CDH12 (0.2, 0.2, 2 Hz), it can be seen that when $f = 2$ Hz, the anchor displacement increases rapidly and linearly with the cycle number. The test for anchor CDH12 (0.2, 0.2, 2 Hz) is stopped at the 526th cycle, corresponding to the accumulated displacement of 23.7 mm, which is close to $0.5D$. Additionally, the accumulated displacement of anchor CDH12 (0.2, 0.2, 0.5 Hz) is only 2.6 mm after 1200 cycles. The results show that the influence of frequency on accumulated displacement is much higher than that of embedment ratio, cyclic amplitude and mean load. Therefore, the safety margin should be increased considering the impact of frequency variations.

Figure 16 indicates that the displacement accumulation rate of anchor CDH12 (0.4, 0.2, 1 Hz) rises rapidly after the third cycle, and reaches 3.77 mm/cycle after 11 cycles. The development for anchor CDH12 (0.2, 0.2, 2 Hz) has the same trend as that for CDH12 (0.2, 0.2, 0.5 Hz), but the displacement accumulation rate in the stable stage is more than six times that of anchor CDH12 (0.2, 0.2, 0.5 Hz).

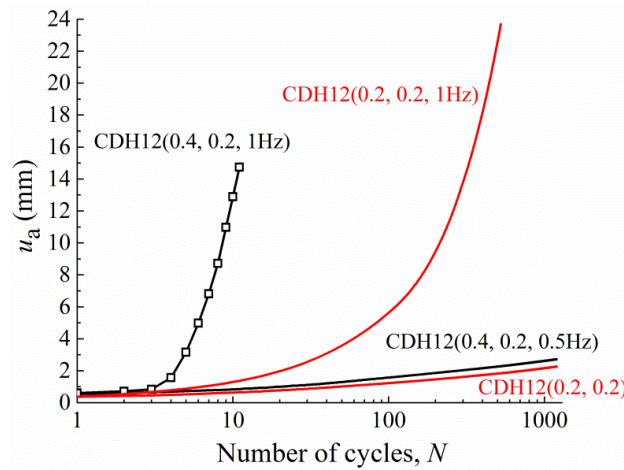


Figure 15. Developments of accumulated displacement under different frequencies.

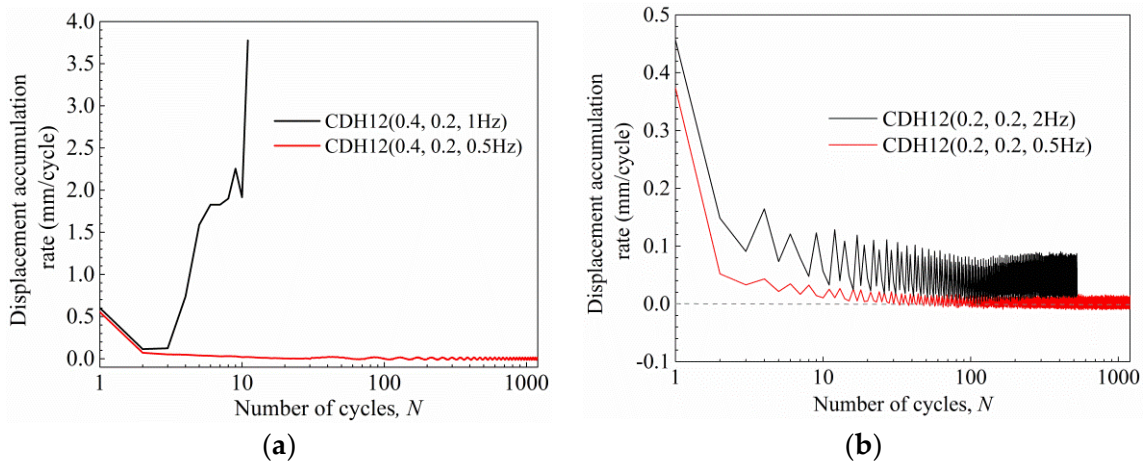


Figure 16. Developments of displacement accumulation rate under different frequencies: (a) $Q_{mean}/Q_t = 0.4$ and $Q_{cyc}/Q_t = 0.2$; (b) $Q_{mean}/Q_t = 0.2$ and $Q_{cyc}/Q_t = 0.2$.

It can be seen from Figure 17 that the development trend of axial stiffness at two frequencies is similar, and the axial stiffness at a high frequency is lower. The stable axial stiffness at a frequency of 0.5 Hz is approximately three times that at frequency of 2 Hz, and the values of stable axial stiffness are about three times those of the initial stiffness.

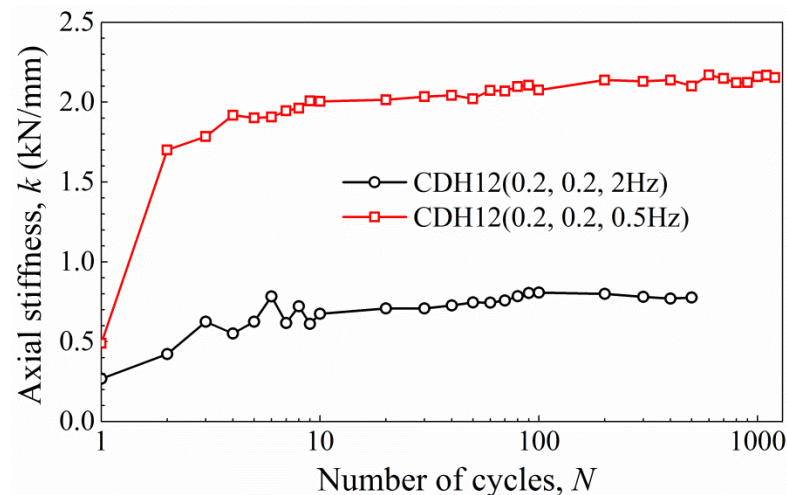


Figure 17. Developments of axial stiffness for different frequencies.

Figure 18 shows the comparisons between the post-cyclic monotonic responses of anchor CDH12 (0.2, 0.2, 0.5 Hz) and CDH12 (0.2, 0.2, 2 Hz) and the monotonic responses without cyclic loading. Their post-cyclic uplift capacity ratios are 0.920 and 1.006, respectively. After cyclic loading, the anchor CDH12 (0.2, 0.2, 2 Hz) produces a large uplift displacement, reaching 0.47D. Although there is a certain loss of embedment depth, the combined effect of vibration frequency and pullout displacement finally densifies the soil above the helix of anchor CDH12 (0.2, 0.2, 2 Hz), and the post-cyclic uplift capacity is not reduced compared with MDH12-5.

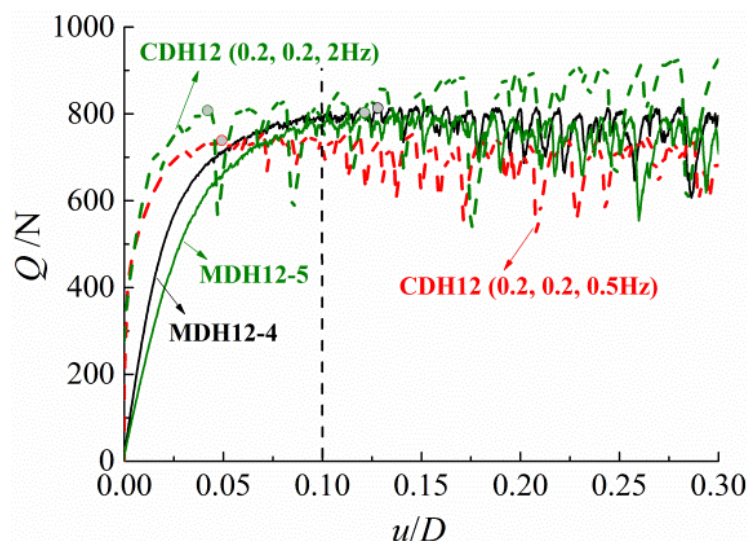


Figure 18. Post-cyclic monotonic and monotonic responses for different frequencies.

3.2. Test Results in Medium-Dense Sand

- Accumulated displacement and axial stiffness

Figure 19 shows the developments of accumulated displacement and displacement rate for the anchors in medium-dense sand under different cyclic parameters. The anchors subjected to a greater amplitude at the same of mean cyclic load produce larger accumulated displacement, which is the same as that in dense sand. The accumulated displacement of anchor CMH12 (0.3, 0.3) is significantly greater than those of anchor CMH12 (0.3, 0.2) and CMH12 (0.3, 0.1) and its pullout displacement after cyclic loading is of 14.1 mm, up to 0.29D, which is far more than 0.1D.

By comparing the accumulated displacement of anchor CMH12 (0.4, 0.2), CMH12 (0.3, 0.2) and CMH12 (0.2, 0.2) with the same amplitude, it is observed that the anchor CMH12 (0.4, 0.2) subjected to the largest mean cyclic load has the largest accumulation displacement within 150 cycles and the largest displacement accumulation rate for the first two cycles, and the accumulated displacement of anchor CMH12 (0.2, 0.2) exceeds that of anchor CMH12 (0.4, 0.2) after 150 cycles, which may be an anomaly caused by the disturbance of sand above the helix or by a large amount of sand back-flowing around the edge of the helix into the void of the helix bottom after being tightly compacted. The accumulated displacement and displacement accumulation rate of anchor CMH12 (0.3, 0.2) are always at the minimum. Therefore, it is discerned that the anchors in medium-dense sand with a greater mean cyclic load may produce larger accumulated displacement when they are subjected to the same medium amplitude. The comparisons among the accumulated displacement of the anchors with the same maximum cyclic load ratio shows that the anchor subjected to a greater amplitude and a smaller mean cyclic load will produce larger accumulated displacement, which is the same as that observed in dense sand.

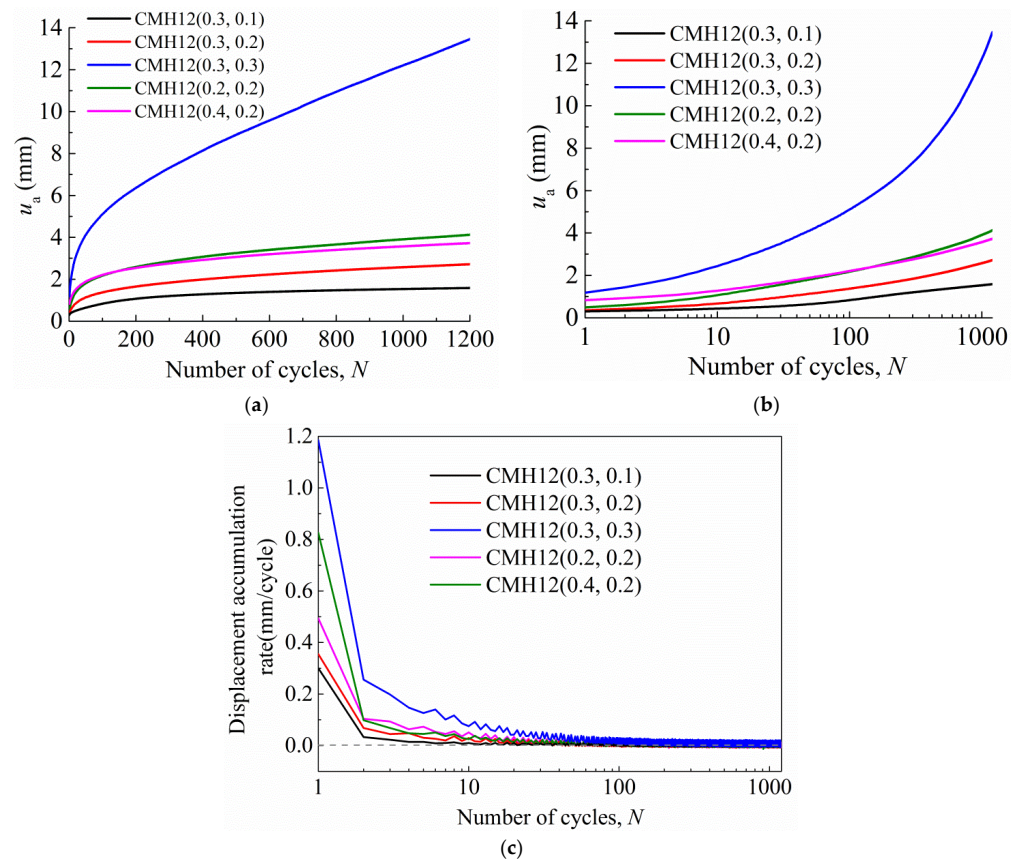


Figure 19. Developments of accumulated displacement and displacement accumulation rates under different cyclic parameters: (a) linear scale of u_a - N ; (b) semi-log scale of u_a - N ; (c) semi-log scale of displacement accumulation rate- N .

Figure 20 shows the development of axial stiffness k under different amplitudes and mean cyclic loads. It can be seen that when the cycle number is not above 3, the k value of each anchor increases rapidly. The axial stiffness of anchor CMH12 (0.3, 0.1) with Q_{cyc}/Q_t of 0.1 becomes stable after 10 cycles, which is the same as that of dense sand. However, for the anchors with Q_{cyc}/Q_t not less than 0.2, it still rises slowly after 10 cycles and becomes steady after 400 cycles. The stable axial stiffness of the anchors with different amplitudes and mean cyclic loads is 3.5–9 times the initial axial stiffness.

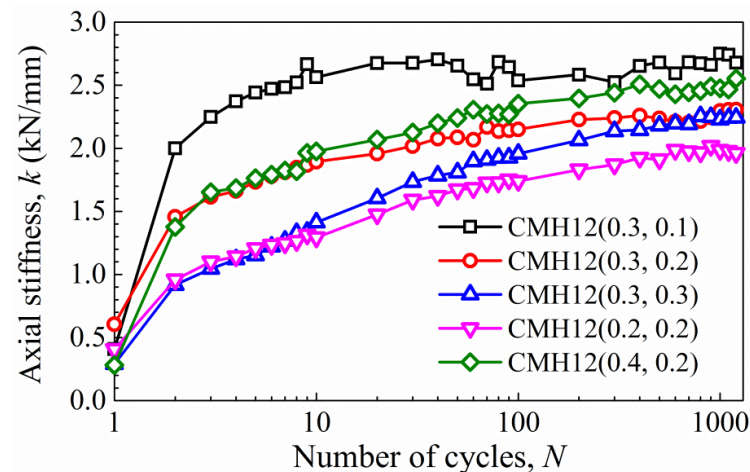


Figure 20. Development of axial stiffness under different amplitudes and mean cyclic loads.

- Post-cyclic monotonic response and uplift capacity

Figure 21 is post-cyclic monotonic and monotonic responses for the anchors in medium-dense sand under different cyclic loading parameters. The post-cyclic monotonic responses for the anchors in medium-dense sand are also stiffer than the monotonic responses without cyclic loading, which is the same as the responses in dense sand. The post-cyclic uplift capacity Q_{pt} of anchor CMH12 (0.3, 0.3) decreases the most, and the ratio β equals 0.827, which may be caused by the flow of sand above the helix to the bottom of the helix loosening the sand above the helix at high amplitudes. The value of β for anchor CMH12 (0.3, 0.1) is 0.866, which is also relatively small compared to other anchors. It indicates that a small amplitude vibration also loosens the sand above the helix. The post-cyclic uplift capacities for the anchors with an amplitude ratio of 0.2 are basically close to the static uplift capacities.

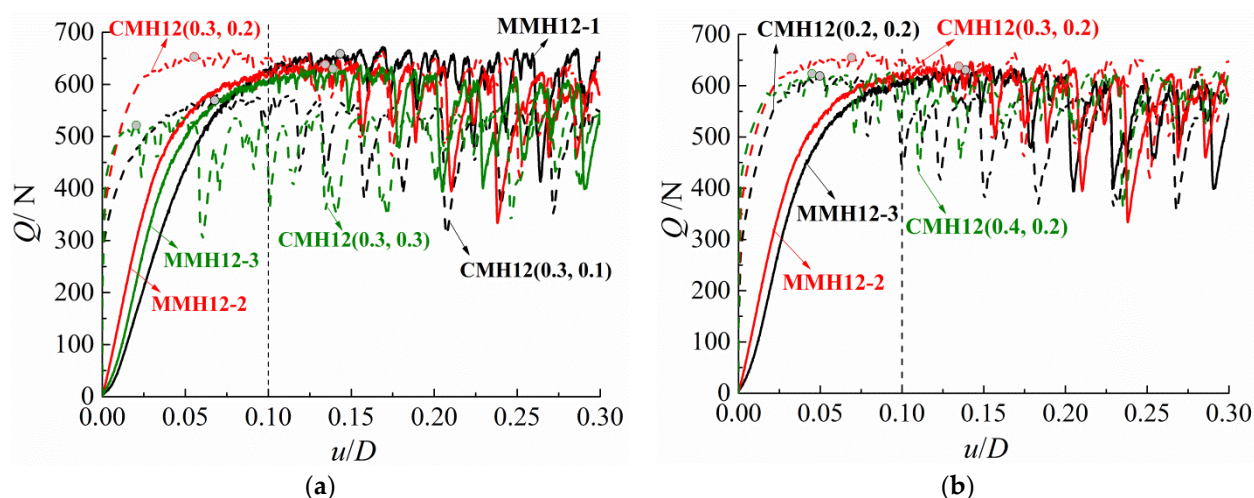


Figure 21. Post-cyclic monotonic and monotonic responses for different cyclic parameters: (a) $Q_{mean}/Q_t = 0.3$; (b) $Q_{cyc}/Q_t = 0.2$.

4. Discussion

The accumulated displacements and post-cyclic uplift capacities for the anchors in medium-dense and dense sands subjected to the same cyclic loading parameters are listed in Table 3. It can be seen that the accumulated displacements of anchors in dense sand are smaller than those in medium-dense sand at the same cyclic loading parameters, and the difference is more obvious when the anchors are pulled under a higher amplitude ratio. The data shown in Table 3 indicate that the smaller the accumulated displacement, the larger the post-cyclic uplift capacity ratio in medium-dense sand, and the trend is opposite in dense sand. Schiavon et al. [17] found that the anchor with the significant capacity degradation after cyclic loading is the one that has a stable cyclic response, and that the anchor with the slight or negligible capacity degradation may be the one that has a meta-stable cyclic response by centrifuge tests of helical anchor in dense sand. This is similar with the observation in dense sand according to which the minimum accumulated displacement does not necessarily lead to high post-cyclic capacity. The post-cyclic uplift capacity ratio of the anchor in dense sand is higher or lower than that in medium-dense sand, which may be related to the flow state of the sand above the helix caused by their accumulated displacements.

The post-cyclic uplift capacities of anchors are affected by the change of sand compactness above the helix and the loss of embedment depth caused by uplift displacement after cyclic loading. Additionally, the change of sand compactness above the helix is controlled by both the uplift displacement after cyclic loading and the amount of sand back-flowing. Lumay et al. [27] considered that the flowability of powders can be evaluated by the measurements of the angle of repose of sand. Schiavon et al. [16] exhibited the gap

formation below the helix during one cycle and Schiavon et al. [17] recognized the upward accumulated displacement being smaller than $5\%D$ at the start of sand flow for the cases of helical anchors in dry dense sand and with the ratio D/d_{50} greater than 275.

Table 3. Accumulated displacement and post-cyclic uplift capacity ratio for anchors in medium–dense and dense sands.

Cyclic Loading $Q_{\text{mean}} \pm Q_{\text{cyc}}$	Sand Compactness					
	Medium–Dense Sand			Dense Sand		
	$u_a(N = 1)$ /mm	$u_a(N = 1200)$ /mm	β	$u_a(N = 1)$ /mm	$u_a(N = 1200)$ /mm	β
$(0.3 \pm 0.3) Q_t$	0.65	13.46	0.827	0.60	5.19	1.094
$(0.4 \pm 0.2) Q_t$	0.83	3.73	0.989	0.55	2.72	0.985
$(0.3 \pm 0.2) Q_t$	0.36	2.72	1.026	0.66	2.52	0.973
$(0.2 \pm 0.2) Q_t$	0.49	4.13	0.984	0.37	2.28	0.920

Figure 22a is the relationship between post-cyclic uplift capacity ratio β and standardized displacement u/D of each anchor after cyclic loading at a frequency of 0.5 Hz. The loss ratios of embedment depth (ratio of uplift displacement to initial embedment depth) of these anchors are all less than 1%. The influence of embedment depth loss on post-cyclic uplift capacity is relatively small, and the influence of soil compactness change may be the control factor. The compactness of the sand above the anchor changes little when the uplift displacement of the anchor is small after cyclic loading, which basically does not affect the subsequent static uplift capacity, such as the test CDH12 (0.5, 0.1). It can be inferred that sand flow starts when the anchor’s upward movement reaches $0.04D$, corresponding to the accumulated displacement $0.0235D$. This is consistent with the conclusion obtained by centrifuge test from Schiavon et al. 2019 [17].

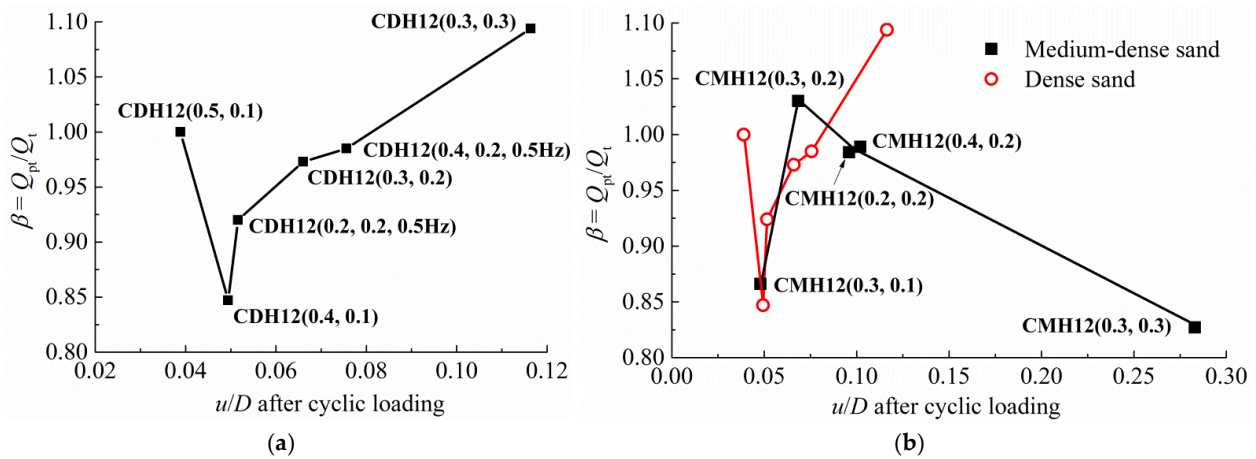


Figure 22. Relationship between u/D after cyclic loading and uplift capacity ratio β . (a) Anchors in dense sand; (b) comparison of anchors in medium–dense sand with those in dense sand.

The sand above the helix gradually becomes loose, which is caused by the backflow of sand with the development of accumulated displacement, and the value of β begins to decrease. When the anchor displacement u reaches $0.05D$ after cyclic loading, the subsequent monotonic uplift capacity Q_{pt} is more than 15% lower than the static uplift capacity Q_t . However, when the accumulated displacement continues to increase, the sand above the helix will be compacted again, and the uplift capacity ratio β will gradually increase. The value of Q_{pt} is close to Q_t when the uplift displacement u exceeds $0.08D$, and even Q_{pt} will be higher than Q_t when uplift displacement after cyclic loading exceeds $0.1D$,

for example, when the post-cyclic uplift capacity of anchor CDH12 (0.3, 0.3) has increased by nearly 10%.

Figure 22b shows the relationship between β and u/D for the anchors in medium-dense sand and the comparison with dense sand. Anchor CMH12 (0.3, 0.1) produces an uplift displacement of $0.05D$ after cyclic loading, corresponding to an embedment depth loss rate of 0.4%. The small embedment depth loss should have a slight influence on the post-cyclic uplift capacity Q_{pt} ; however, the value of Q_{pt} reduces by more than 13%, which indicates that cyclic vibration loosens the sand above the helix of anchor CMH12 (0.3, 0.1). Therefore, it is inferred that the sand above the helix may also flow into the gap at the bottom of the helix in the case that the anchor in medium-dense sand produces a small displacement under cyclic loading. Additionally, when the uplift displacement after cyclic loading of anchor CMH12 (0.3, 0.2) is greater than $0.07D$, the sand above the anchor recovers to the pre-vibration state or is densified, and thus Q_{pt} reaches the static uplift capacity Q_t , or an even higher magnitude. However, when the uplift displacement continues to increase, the sand on the helix is pulled tight enough to cause more sand flowing back to the helix's bottom gap, and the sand above the helix becomes loose again, such as for the anchors CMH12 (0.4, 0.2), CMH12 (0.2, 0.2) and CMH12 (0.3, 0.2).

It can be seen from Figure 22b that the variation rule of the post-cyclic uplift capacity ratio in medium-dense sand with the standardized uplift displacement is different from that in dense sand. When the uplift displacement caused by vibration is about $0.05D$, the compactness of the sand above the helix in medium-dense sand and dense sand will be looser than that before cyclic loading. With the continuous increase in uplift displacement after cyclic loading, the sand above the helix returns to the initial state before vibration, and the uplift displacement required for medium-dense sand to return to the initial state is smaller than that of dense sand. However, the post-cyclic uplift capacity ratio of anchor in dense sand continues to increase with the increase in uplift displacement after cyclic loading. After the uplift displacement exceeds $0.1D$, Q_{pt} still improves, indicating that the sand above the helix in dense sand is less likely to flow back to the bottom of the helix than that in medium-dense sand.

5. Conclusions

A series of reduced-scale cyclic loading model tests of a single-helix anchor in sand with different compactness have been carried out, and the effects of anchor embedment ratio and cyclic loading parameters on the accumulated displacement, the development of axial stiffness and the post-cyclic monotonic uplift capacity have been analyzed. The correlation of post-cyclic monotonic uplift capacity ratio and post-cyclic displacement and possible influence of the cyclic uplift displacement of the anchors on the sand flow above the helix were discussed. The main conclusions are as follows:

- The single-helix anchor in dense sand with an optimal embedment ratio that is determined according to the relationship between breakout factors and embedment ratio under monotonic loading still exhibits a relatively high uplift capacity after cyclic loading. The post-cyclic monotonic responses of all the anchors exhibit stiffer behaviors.
- The anchors in both dense sand and medium-dense sand subjected to greater amplitude ratios will produce greater accumulated displacement when the same frequency and mean cyclic load ratio are applied. The influence of the mean cyclic load ratio on the accumulated displacement of anchors in dense sand may be affected by the amplitude. Under the same medium amplitude ratio, the anchor in dense sand subjected to a greater mean cyclic load ratio will produce a larger accumulated displacement, which is similar to the anchor in medium-dense sand. Additionally, for the case of anchors with the same small amplitude in dense sand, the influence of the mean cyclic load ratio on the accumulated displacement is opposite. The cyclic frequency has the greatest influence on the accumulated displacement, and the influence of cyclic amplitude is relatively greater than that of the mean cyclic load ratio. For the anchors in both dense sand and medium-dense sand under the same maximum cyclic load

ratio Q_{\max}/Q_t , the greater accumulated displacement is obtained when the anchors are subjected to a larger value of Q_{mean}/Q_t and a smaller value of Q_{cyc}/Q_t .

- There are some differences in the development of axial cyclic stiffness of single-helix anchors in medium–dense sand and dense sand. When the anchors in medium–dense sand are subjected to a small amplitude, the development between axial stiffness and cycle number is the same as that of dense sand, and axial stiffness tends to stabilize at 10 to 50 cycles. However, the axial stiffness of the anchors in medium–dense sand with a medium amplitude still rises slowly after 10 cycles, and becomes stable after 400 cycles. The ratio of stable axial stiffness and initial value of anchors in dense sand is between 3 and 6, and the ratio varies between 3.5 and 9 in medium–dense sand.
- The accumulated displacements at the first cycle and after cyclic loading in dense sand for the anchors under the same standardized cyclic load parameters are basically smaller than those in medium–dense sand, indicating that the anchor in dense sand has higher pullout resistance.
- The backflow of sand above the helix has been inferred by analyzing the relationship of post-cyclic uplift capacity ratio and uplift displacement after cyclic loading. The variation of the post-cyclic uplift capacity ratio in medium–dense sand with the standardized uplift displacement is different from that in dense sand. However, the compactness of sand above the helix both in medium–dense sand and dense sand will be much looser than that before cyclic loading at the uplift displacement of $0.05D$ after cyclic loading. This relationship of post-cyclic capacity with anchor upward movement in dense sand and medium–dense sand can provide the reference of evaluation of stability and bearing capacity of helical anchors.

This investigation on the cyclic behavior of single-helix anchors in dense sand and medium–dense sand was carried out based on small scale model tests; therefore, the results may be different from those from field tests and centrifuge tests. In addition, the cyclic frequency and cyclic load parameters are selected based on the wind load on the transmission tower. Therefore, further studies are required to provide more comprehensive and conclusive observations.

Author Contributions: Conceptualization, formal analysis, and writing—review and editing, D.H. and R.C.; investigation and writing—original draft preparation, J.C. and X.Z.; investigation and data curation, C.Y. and X.C. All authors have read and agreed to the published version of the manuscript.

Funding: This research was funded by National Natural Science Foundation of China grant number 52078108, Jilin Province Youth Science and Technology Innovation Leader and Team Project of Provincial Department of Science and Technology Grant number 20210509058RQ and Scientific Research Project of Jilin Provincial Department of Education Grant number JJKH20210103KJ.

Institutional Review Board Statement: Not applicable.

Informed Consent Statement: Not applicable.

Conflicts of Interest: The authors declare no conflict of interest.

References

1. Spagnoli, G.; Tsuha, C.D.C. A review on the behavior of helical piles as a potential offshore foundation system. *Mar. Georesources Geotechnol.* **2020**, *38*, 1013–1036. [\[CrossRef\]](#)
2. Tsuha, C.H.C.; Aoki, N.; Rault, G.; Thorel, L.; Garnier, J. Evaluation of the efficiencies of helical anchor plates in sand by centrifuge model tests. *Can. Geotech. J.* **2012**, *49*, 1102–1114. [\[CrossRef\]](#)
3. Merifield, R.S. Ultimate uplift capacity of multiplate helical type anchors in clay. *J. Geotech. Geoenviron. Eng.* **2011**, *137*, 704–716. [\[CrossRef\]](#)
4. Lutenecker, A.J. Behavior of multi-helix screw anchors in sand. In Proceedings of the 2011 Pan-Am CGS Geotechnical Conference, Toronto, ON, Canada, 2–6 October 2011.
5. Feng, S.J.; Fu, W.D.; Chen, H.X.; Li, H.X.; Li, J. Field tests of micro screw anchor piles under different loading conditions at three soil sites. *Bull. Eng. Geol. Environ.* **2021**, *80*, 127–144. [\[CrossRef\]](#)
6. Cerfontaine, B.; Knappett, J.; Brown, M.; Davidson, C.; Sharif, Y. Screw Pile Design Optimisation under Tension in Sand. In Proceedings of the ECSMGE 2019, Reykjavik, Iceland, 1–6 September 2019.

7. Ding, H.; Wang, L.; Zhang, P.; Liang, Y.; Tian, Y.; Qi, X. The recycling torque of a single-plate helical pile for offshore wind turbines in dense sand. *Appl. Sci.* **2019**, *19*, 4105. [[CrossRef](#)]
8. Clemence, S.P.; Smithling, A.P. Dynamic uplift capacity of helical anchors in sand. In Proceedings of the 4th Australia–New Zealand Conference on Geomechanics, Perth, WA, Australia, 14–18 May 1984.
9. Cerato, A.B.; Victor, R. Effects of helical anchor geometry on long-term performance of small wind tower foundations subject to dynamic loads. *J. Deep. Found. Inst.* **2008**, *2*, 30–41. [[CrossRef](#)]
10. Cerato, A.B.; Victor, R. Effects of long-term dynamic loading and fluctuating water table on helical anchor performance for small wind tower foundations. *J. Perform. Constr. Facil.* **2009**, *23*, 251–261. [[CrossRef](#)]
11. Buhler, R.; Cerato, A.B. Design of dynamically wind-loaded helical piers for small wind turbines. *J. Perform. Constr. Facil.* **2010**, *24*, 417–426. [[CrossRef](#)]
12. Sharnouby, M.M.E.; Naggar, M.H.E. Field investigation of axial monotonic and cyclic performance of reinforced helical pulldown micropiles. *Can. Geotech. J.* **2012**, *49*, 560–573. [[CrossRef](#)]
13. Sharnouby, M.M.E.; Naggar, M.H.E. Axial monotonic and cyclic performance of fibre-reinforced polymer (FRP)—Steel fibre-reinforced helical pulldown micropiles (FRP-RHPM). *Can. Geotech. J.* **2012**, *49*, 1378–1392. [[CrossRef](#)]
14. Newgard, J.T.; Schneider, J.A.; Thompson, D. Cyclic response of shallow helical anchors in a medium dense sand. In Proceedings of the 3rd Conference on Frontiers in Offshore Geotechnics, Oslo, Norway, 10–12 June 2015.
15. Wada, M.; Tokimatsu, K.; Maruyama, S.; Sawaishi, M. Effects of cyclic vertical loading on bearing and pullout capacities of piles with continuous helix wing. *Soils Found.* **2017**, *57*, 141–153. [[CrossRef](#)]
16. Schiavon, J.A.; Tsuha, C.H.C.; Thorel, L. Cyclic and post-cyclic monotonic response of a single-helix anchor in sand. *Géotechnique Lett.* **2017**, *7*, 11–17. [[CrossRef](#)]
17. Schiavon, J.A.; Tsuha, C.H.C.; Neel, A.; Thorel, L. Centrifuge modelling of a helical anchor under different cyclic loading conditions in sand. *Int. J. Phys. Model. Geotech.* **2019**, *19*, 72–88. [[CrossRef](#)]
18. Schiavon, J.A.; Tsuha, C.; Thorel, L. Monotonic, cyclic and post-cyclic performances of single-helix anchor in residual soil of sandstone. *J. Rock Mech. Geotech. Eng.* **2019**, *11*, 824–836. [[CrossRef](#)]
19. Thorel, L.; Haffar, I.E.; Maatouk, S.; Schiavon, J.A.; Tsuha, C. Cyclic loading of helical pile as anchor for floating wind turbines: Centrifuge tests. In Proceedings of the ISFOG2020, Austin, TX, USA, 28 August 2022.
20. Hao, D.X.; Chen, R.; Yuan, C.; Kong, G.Q.; Shi, D.D. Centrifugal model tests on cyclic uplift performance of wished-in-place helical anchors in dense sand. *Chin. J. Rock Mech. Eng.* **2021**, *40*, 2896–2904. (In Chinese)
21. Product drawings and ratings. In *Technical Design Manual*, 4th ed.; Hubbell Power Systems Inc.: Columbia, SC, USA, 2018; pp. 7-31–7-62.
22. Hao, D.X.; Wang, D.; O’Loughlin, C.D.; Gaudin, C. Tensile monotonic capacity of helical anchors in sand: Interaction between helices. *Can. Geotech. J.* **2019**, *56*, 1534–1543. [[CrossRef](#)]
23. Ilamparuthi, K.; Dickin, E.A.; Muthukrisnaiah, K. Experimental investigation on the uplift capacity of circular anchors in sand. *Can. Geotech. J.* **2002**, *39*, 648–664. [[CrossRef](#)]
24. Hao, D.X.; Chen, R.; Fu, S.N. Experimental study on uplift capacity of multi-helix anchors in sand. *Chin. J. Geotech. Eng.* **2015**, *37*, 126–132. (In Chinese)
25. Hanna, T.; Sivapalan, E.; Senturk, A. The behaviour of dead anchors subjected to repeated and alternating loads. *Ground Eng.* **1978**, *11*, 28–34. [[CrossRef](#)]
26. Petereit, R. The Static and Cyclic Pullout Behavior of Plate Anchors in Fine Saturated Sand. Master’s Thesis, Oregon State University, Corvallis, OR, USA, 1987.
27. Lumay, G.; Boschini, F.; Traina, K.; Bontempi, S.; Remy, J.C.; Cloots, R.; Vandewalle, N. Measuring the flowing properties of powders and grains. *Powder Technol.* **2012**, *224*, 19–27. [[CrossRef](#)]